Volumetric Bit-Wise Optical Data Storage for Space Applications

T. D. Milster*, Y. Zhang*, J. Butz*, Tim Miller*, Taeyoung Choi*, Warren Bletscher*, David Felix*, Fung-Hsu (Geoffrey) Wu***, E. P. Walker***

*Optical Sciences Center
University of Arizona
Tucson, Arizona 85742
milster@arizona.edu

**Institute of E-O Engineering
National Chiau-Tung University
Hsin-Chu, Taiwan

***Call/Recall, Inc.
6160 Lusk Blvd., Suite C-206
San Diego, CA 92121

ABSTRACT

Volumetric bit-wise optical memory is a revolutionary technology that has the benefits of lower cost (tens of dollars/Gbit), low risk, and an order of magnitude smaller size and mass than other memory technologies. Our research centers on constructing an Advanced Engineering Model (AEM) of a memory device that has the potential to be used in space applications. A new servo system is designed and tested for controlling the position of a laser beam in the volumetric media. A master laser beam at wavelength A is guided on the media by focusing it onto a compact-disc like groove structure. A slave laser beam at wavelength B follows the master beam, but at a different depth in the volumetric recording material, where writing and reading occurs. In addition to building the AEM, several tests have been performed on a plastic-based volumetric photochromic media with respect to proton radiation and high-energy particle sensitivities. A second test stand is under construction that will evaluate the potential for volumetric recording in a new system geometry. Our work estimates that effective areal densities of over $3Tb/in^2$ are practical with the new geometry, and high data rates are possible with a new wavelength multiplexing scheme.

I. INTRODUCTION

Instead of recording only on a plane, bits in a volumetric storage device are stored throughout the volume of the material in multiple planes. The volumetric storage element has dimensions of the writing/reading laser wavelength. With a wavelength of 650 nm, this report shows that effective surface density of over one terabit per cubic inch is possible.

We are investigating and characterizing a volumetric optical memory device based on a class of light-absorbing (photo-chromic) compounds that when exposed to laser light absorb photons two at a time and trigger chemical and physical changes (such as fluorescence) with micrometer-sized resolution in three dimensions.

Our activities aim at enabling the Earth Science Enterprise (ESE) to integrate large global data sets involving space based observation systems. With many space and ground-based sensors, ESE must acquire, process, and deliver huge volumes of data. These remote sensing and related data will help solve problems such as global change, environmental monitoring, agricultural inventory, etc.[1] The amount of data to be collected and processed per satellite runs into terabytes.

Development of adaptive, high capacity, high data rate optical storage for space vehicles can set an infusion path by establishing a realistic on-board storage platform for such data organization technologies as feature extraction and data prioritization for transmission. The impact of establishing reliable ultra high capacity storage can also significantly influence development of hierarchical data segments and reduction in data volume for downlink. Terabyte capacity on-board optical storage is an ideal platform on which generations of data products for direct distribution to users can be made possible.

Our last report discusses the Arizona Readout Test

Stand (ARTS), media testing with respect to temperature sensitivity, optical system considerations, and an introduction to the Advanced Engineering Model (AEM) for volumetric optical storage.[2] The following sections provide a snapshot of our current research progress, which includes characterizing materials for space environments and development of the AEM. Section 2 provides background on the photochromic process. Section 3 describes recent progress with the AEM, which includes an improved master/slave servo system. Section 4 describes media testing results with respect to heavy ion and proton radiation. Section 5 describes a new test stand that is configured for testing volumetric media samples. Section 6 details work in the volumetric data channel, which includes diffraction simulations of inter-layer crosstalk and focus sensitivity, advanced lens design that predicts up to 3.3 Tb/in^2 effective surface density, and a new technique for providing multiple beams for increased data rate. Section 7 summarizes our conclusions.

II. BACKGROUND ON THE PHOTOCHROMIC PROCESS

With a tightly focused laser beam, the photochromic process is initiated and controlled within micrometer-size spaces. A data mark is written within the volume only at points of sufficiently high irradiance.[3,4,5] At these points, two-photon absorption occurs, resulting in a bond dissociation. Thus, the molecular structure is changed into a new, 'written', molecule with a different absorption and emission spectrum, as shown in Fig. 1. To "read" the information written within the volume, the approach exploits the fact that the written form absorbs at longer wavelengths than the unwritten form. As shown on the right side of Fig. 1, excitation of written molecules is followed by fluorescence at ~660 nm, which returns the molecule to its ground state. The presence or absence of this fluorescence is detected and classified as a physical '1' or '0' for the stored data mark. Since the decay lifetime is ~5 nanoseconds and the concentration of molecules is high, it is possible to excite the written molecules many times in a single read cycle and increase the total light collected at the detector.

The advantage of a 2-photon absorption process is based upon its ability to selectively excite molecules inside a volume without populating molecules on the surface of the device. This may be achieved because the laser photons have less energy than the energy gap between the ground state and first allowed electronic level. Therefore, photons propagate through the medium without being absorbed by a one-photon process. However, in the vicinity of the laser beam focus, the intensity is high enough so that two photons can combine to excite carriers across the energy gap. The transition probability of a 2-photon absorption process partly depends upon the temporal and spatial confinement of the photons of the recording laser irradiance, so lasers emitting high peak power in short pulses, i.e. picosecond and sub-picosecond pulses, are used.

The recording material is dispersed in a polymer host, which can then be shaped to produce disks with integrated structures for alignment and mounting. This project uses 25mm x 3mm PMMA disks with homogeneously dispersed storage materials. Polymerization molding, compression molding and polishing have been utilized to produce the desirable optical quality polymer for 3D optical memory disks.

A representation of the disks we use is shown in Fig. 2, where other technologies are also shown for comparison. Our 25 mm diameter test samples, if used with 500 layers and 1 Gbyte per layer, can produce a disk containing 500 Gbytes. With parallel readout beams, high data rate retrieval is also achieved.[6]

III. THE ADVANCED ENGINEERING MODEL

The Advanced Engineering Model (AEM) is a sophisticated test stand for characterizing volumetric media and testing design concepts for space applications.[2] The AEM allows for both reading and writing of bits in two-photon volumetric media, and applies a novel tracking system to solve the problem of tracking inside homogeneous volumetric media. The AEM is shown in Fig. 3. It is configured with mostly off-the-shelf optical components.

Conventional optical data storage devices require a closed-loop servo system to keep the laser spot sufficiently locked onto the data track being read or written to, in order to compensate for errors in the laser spot position.[7] This servo requires some pre-existing reference track or features to follow, which are not present in unwritten homogeneous volumetric media. The AEM uses a "slave-servo" method to implement tracking inside blank media. The slave-servo method has the advantage of providing tightly-spaced tracks and a high data density, while using convenient and economical media that do not require complicated multi-layer structures. This servo

method should help overcome difficulties discovered in temperature stability with the polymer host.[2]

In this method, the medium is mounted rigidly to a master grooved disk, *e.g.* a commercial CD, so that both disks rotate together on a common axis. A closed-loop servo system is coupled to the CD, the "master disk", and a particular track is followed. When track lock is achieved, this lock is coupled to a slave system that controls a write/read beam for the medium. The write/read beam thus traces a path inside the medium that replicates the track followed by the master servo loop. With this system, any positioning errors in the medium/disk pair as it rotates (repeatable or non-repeatable) are tracked by the master feedback system. Since the medium and the master disk are rigidly fixed together and have corresponding position errors, the position of the laser spot in the medium is well controlled. A separate track offset driver moves the write/read beam focus by constant amounts, in order to define multiple tracks within the width and depth of the medium.

There are several possible configurations for the AEM that implement the slave-servo concept. Initial experiments use a "sandwich" configuration, in which the media and master disk are sandwiched together. Two separate actuators are used: the master actuator locks onto the CD-R tracks, and the slave actuator writes and reads to the medium, driven by the master servo loop. This version of the AEM is designed to be compact and economical, using several off-the-shelf components.

With the sandwich configuration, bits are reliably written in a two-photon volumetric medium sample, which is a 25-mm diameter and 3-mm thick disk. Multiple tracks are also written at controlled depths and radii inside the media volume, as shown in Fig. 4. The bits are of the size and shape predicted by theory (2 x 6 x 20 microns). Readout of the bits is successful, with a written 2T pattern being read back with a carrier-to-noise ratio (CNR) of 37dB.

However, the two-actuator sandwich configuration suffers from slave control problems, such that written tracks cannot be read consistently. The open-loop slave tracking servo lacks immediate feedback control for system errors, and therefore proves susceptible to long-term drift, vibration, and component mismatching.

A more robust design, which is called the "two-in-one" configuration is now under development. This configuration combines the tracking beam and the write/read beams through a single actuator, as shown in Fig. 5. This design removes the open-loop difficulties of the sandwich configuration, and thus minimizes susceptibility to system errors. Using adjustable compensation optics, the write/read beam is focused through the same actuator lens to different layers in the disk pair. The AEM redesign includes new mechanical parts and appropriate modifications to the electronics.

The optical design requirements for the two-in-one configuration are more substantial than in previous configurations, since several wavelengths are folded into the same path. These requirement include: 1) a design that works over a wide range of wavelengths from 532 nm to 780 nm; 2) simultaneous control of multiple wavelengths; 3) adjustability to control the focus depth of both the write and read beams; and 4) control of aberration in all cases to allow tight laser focus spot sizes. Initial designs show that spherochromatism is the dominating problem in an uncorrected system.

The wavelength range problem is solved by placing a diffractive optical element (DOE) before the objective lens. This DOE has several advantages over refractive solutions. First, DOEs have negative chromatic dispersion, which is used to counteract positive dispersion in the objective. Secondly, the DOE is concurrently designed to correct for system spherical aberration. Thirdly, adjustment of writing and reading depth in the medium is achieved by moving only a single external lens element. Use of a DOE leads to diffraction-limited performance over a 200-micron range of focus depths for writing and reading in the two-photon medium with otherwise commercially available lenses. Given the numerical aperture of the Geltech 340080 objective lens, this range of depths allows for up to ten written layers with excellent bit quality. More advanced designs allow for larger depth ranges.[8,9] Modeling results indicate reasonable alignment tolerances of the optical design (the DOE, the adjustable telescope, beam coalignment) in the two-in-one configuration.

Unfortunately, DOEs are not commercially available off-the-shelf, and custom DOEs cost several thousand dollars. Therefore, an in-house lithography technique is implemented in order to fabricate a grayscale kinoform, which is a transmission phase grating made out of photoresist on a glass substrate. This procedure is economical with standard lithography equipment and collaboration with a local commercial printing business.[10] First, the DOE image is designed using mathematical software. Next, the printing business transfers the digital image

to a film negative using a commercial slide imager. Then, a simple optical system projects a minified image of the negative onto photoresist. After the photoresist is exposed and developed, it is ready for testing and use. Nonlinearities in the process of film creation and development/exposure typically produce incorrect DOE profiles, so it is necessary to precorrect the grayscale of the original computer image over several iterations of the process. Several DOEs are successfully fabricated using this procedure. However, diffraction efficiency into the desired diffraction order is still relatively low, and more iterations of the procedure are necessary.

The AEM is proven to be a useful test stand for writing and reading bit tracks in homogeneous volumetric media. The slave-servo concept shows great promise for writing reliable, densely-spaced tracks. The single-actuator two-in-one configuration allows consistent tracking without susceptibility to long-term drift, environmental conditions, or mismatched system components. Other test stands are also under development, like the one shown in Fig. 6.[11]

IV. MEDIA TESTING

The robustness of a two-photon disk in a radiation environment is critical if a volumetric data storage system with this media is used in space flight. Hence, experiments are conducted to test samples exposed to heavy ion radiation and proton radiation. These results complement previously reported temperature studies.[2]

The first set of experiments is media testing under the influence of heavy ion radiation, which is conducted under contract at Brookhaven National Lab's Tandem Van de Graaff accelerator facility. In this test, photo-chromic disks are exposed to six different heavy ions: I-126 (350 MeV), Br-81 (290 MeV), Ni-58 (260 MeV), Cl-35 (210 MeV), Mg-24 (170 MeV), F-19 (140 MeV).[12] The penetration ranges of these particles are from 45 micron to 200 micron. Table 1 shows test results. We conclude that the heavy ions have no effect on the disk performance due to the fact that the data layer is 1.2 mm below the front surface of the disk, and heavy ions can not penetrate the substrate material deeply enough to reach the data layer.[13]

The second set of experiments is media testing under the influence of proton radiation, which is conducted under contract at UC Davis Crocker Nuclear Laboratory. In this test, twenty-four disks are tested after their exposure to 30 Mev and 60 Mev level proton radiation.[14] Radiation flux is 1e6 p/cm^2-s and 1e9 p/cm^2-s, and the total radiation periods are 10 s, 50 s and 100 s. Test results are shown in Table 2. This experiment shows that high-flux proton radiation exposes all dye molecules inside the disk. Hence, the information in a disk is lost. We conclude that the 30 Mev and 60 Mev proton beam at 1e9 p/cm^2-s flux rate erases data in a short amount of time. Since the optical storage device is commonly deep inside the satellite, we expect that the satellite itself can provide a shielding environment for the photo-chromic disk.

V. NEW TEST STAND FOR COUPON SAMPLES

Coupon samples are typically the first iteration of new media designs, even though they are eventually made into disks. Dynamic testing is expensive, because a complete disk and associated readout head must be developed before real dynamic performance is evaluated. Under development is a shortcut that allows dynamic testing on coupon samples. The new test stand uses a spinning objective lens. The coupon sample remains static. Data patterns are written and read within a small linear range on the coupon, which is designated as Δx. The other important parameter is focus sensitivity Δf, which is the depth between the perfect focus plane and the focus plane at the limit where data marks are just written successfully.

The test stand setup is shown in Fig 7. This test stand is designed to perform both writing and reading on coupon samples. The laser wavelength is 650nm, although other lasers are easily incorporated. The collimated linear-polarized laser beam first passes through a polarized beam splitter and relay telescope 1, which is made of two 100mm focal length achromatic lenses. The polarization of the beam is changed to circular after it passes through a quarter wave plate. Then, relay telescope 2,which is made of two 200mm focal length achromatic lenses, delivers the beam to a glass aspherical lens (Geltech 350390) with NA of 0.68. This objective lens serves as system stop and focuses the laser beam onto the sample. A spherical aberration compensator is necessary for some samples. One compensation method is to use a liquid crystal compensator, which is mounted in pupil plane 1, to compensate up to two waves of spherical aberration. Note that the pupil plane 1 is conjugate to the stop plane. A second method is to change the distance between the two lenses in relay telescope 2

to compensate induced spherical aberration.[8,9] It is obvious that both methods can be combined together to achieve greater compensation range. In the reading process, the reflected laser beam from the sample is focused by a lens, which is mounted in pupil plane 2, onto a detector. Note that pupil plane 2 is also conjugate to the stop plane. Figure 8 shows the optical head and the position of a media sample.

Results from two samples are reported that illustrate differences in behavior for volumetric applications. Table 3 and Table 4 list experimental results for sample 1 and sample 2, respectively. Results show that the minimum power required for the two samples increases as the focus spot speed and data rate increase. Δx equals to 500 μm and 50 μm for sample 1 and sample 2, respectively. The experimental settings to find Δx are focus spot speed = 2m/s, data rate = 500 kHz, output laser power = 4 mW for sample 1; while focus spot speed = 1m/s, data rate = 250 kHz, output laser power = 14 mW for sample 2. Note that the minimum powers required in the writing process for sample 1 and 2 are 2.5 mW and 12 mW, respectively. As the focus moves away from the perfect focus spot, the irradiance on the coupon sample falls below the irradiance threshold within a shorter range for sample 2 than for sample 1, which leads to smaller Δx in sample 2. Δf 's equal ± 7 μm and ± 2 μm for sample 1 and sample 2, respectively.

VI. DATA CHANNEL DEVELOPMENT

Inter-Layer Crosstalk and Focus Sensitivity

Inter-layer crosstalk, which is the amount of signal from an adjacent layer that is detected while scanning a layer of interest, is the most important factor that limits layer spacing T_z. It's well known that a small detector in a confocal read out system reduces the inter-layer crosstalk, but the small detector also limits the detected signal and leads to signal-to-noise-ratio (SNR) reduction. Hence, impact of detector size on inter-layer crosstalk and SNR in a fluorescent system is discussed in this section by using the physical-optics-based software OPTISCAN, which is described in previous reports.[15,16] Dependence of crosstalk and focus sensitivity are studied with two sets of simulations. Focus axial position and layer spacing are parameters. Cartesian axes define (x, y) as the transverse recording plane and z as the focus dimension.

Figure 9 shows mark patterns used to simulate inter-layer crosstalk in the first set of calculations. Rectangular marks in layers 1 and 3 have recording-plane mark sizes L_x=L_y=1 μm with 50% duty cycle (recording-plane mark periods T_x=T_y=2μm). Marks in layer 2 have L_x=L_y=0.5μm with 50% duty cycle (T_x=T_y=1μm). For all layers, mark depth L_z=0.9 μm. This particular combination of a high-frequency pattern sandwiched between two low-frequency patterns is analogous to the worst-case crosstalk condition in a single layer, where a high-frequency track lies between two low-frequency tracks.[17] In this simulation, both confocal (v_d =0.9) and non-confocal(v_d =8) systems are considered. v_d is defined as the normalized detector radius:

$$v_d = \frac{2\pi r_d}{ms}, \qquad \text{(Eq. 1)}$$

where r_d is the physical detector radius and m=3.85 is the transverse magnification of the system. Full-width-at-1/e^2 spot size s=λ/NA, where λ is the laser wavelength and NA is the numerical aperture of the optical system. NA equals to $n\sin\theta$, where n is the refractive index in image space and θ is the marginal ray angle in image space. The volume of a *basic cell* is defined as $V_{basic} = s^2 \times \frac{n\lambda}{NA^2}$.

Simulation shows that for the confocal system, a conservative choice for $T_z - L_z = \Delta b$ might be Δb=2.5 μm, with acceptable focus offset from the top of the data layer Δz between Δz=0 μm and Δz=0.80 μm. At this operating point, the system exhibits an additional –4 dB of crosstalk rejection beyond the standard –30 dB criterion. For Δb=2.5 μm, T_z=3.4 μm, which is 1.31 times greater than the depth of a basic cell. For a non-confocal system with a crosstalk rejection of –34 dB, T_z must be around 5.7 μm (Δb = 4.8 μm) for acceptable crosstalk performance, which is 2.2 times greater than the depth of a basic cell. γ is defined as T_z / (the depth of the basic cell). For both far-field system and near-field system, γ is around 1.33 for a confocal geometry, and γ is around 2.4 for a non-confocal geometry.

Although the confocal system shows good crosstalk rejection, a compromise system with slightly higher v_d gives good crosstalk rejection and high signal-to-noise ratio (SNR). Figure 10 shows the crosstalk level and SNR versus v_d when $\Delta z = 0.45$ μm and $\Delta b = 3.0$ μm. The crosstalk level, which is represented by dashed line, increases

as pinhole size increases, which is expected. The SNR, which is represented by the solid line, increases dramatically as v_d increases from 1 to 3 and becomes saturated with further increase of v_d. The optimum value is v_d = 3, where SNR is just at saturation and crosstalk is –30 dB.

The second set of simulations determines acceptable focus offset when an objective lens scans through an isolated layer with NA=0.6. Acceptable focus offset Δz_0 is defined as the distance between the center plane of the marks and the focal plane Δz where SNR drops by 3 dB compared to its maximum value. Simulation results are presented in Table 5. The SNR of a confocal system is generally 7 dB lower than a non-confocal system. Δz_0 is longer than the mark depth in both confocal and non-confocal systems. The non-confocal system has a looser tolerance for focus (larger $\Delta z_0 / L_z$) compared to a confocal system. Results also show that bigger marks result in higher SNR, which is expected, because more light is generated by a larger mark that is then collected by the detector.

Advanced Lens Design

Simple aspheric lenses used for single-layer optical data storage systems do not work well for volumetric data storage technology, due to spherical aberration generated by the focus moving through different layers inside the recording medium.[4] In this section, far-field and near-field systems with proper spherical aberration compensator and their performance are discussed.

The example far-field system of uses a 0.6 NA objective lens. Since multiple layers in the medium are treated as stacked plane parallel plates, shifting focus from one layer to another induces spherical aberration ΔW_{040}, in the form

$$\Delta W_{040} = -\frac{1}{8} \times \left[\frac{n^2 - 1}{n^3} \right] \times NA^4 \times N \times T_z \,. \quad \text{(Eq.2)}$$

An effective surface density Π is defined as

$\Pi = N$ / mark surface area, (Eq. 3)

where N is the number of layers that are processed. Therefore, Π of a far-field read out system is

$$\Pi = \frac{1}{L_x L_y} N = \frac{8(\Delta W_{040})_{\max} n^2}{\gamma \lambda^3 \left(n^2 - 1 \right)} \text{ Gb/in}^2, \quad \text{(Eq. 4)}$$

where $(\Delta W_{040})_{\max}$ and λ have units of microns. Notice that Eq. (4) is not a function of NA. That is, the effective surface density of a far-field volumetric system is, to first order, not a function of NA. Figure 11 (a) shows the layout of this system. The overall length is 13 mm and maximum field angle is 0.5 degree. After changing d_{focus} for moving focus d_{layer} through media layers, d_{comp} is adjusted for the purpose of spherical aberration compensation. This study indicates this design compensates up to $(\Delta W_{040})_{\max} / \lambda$ =36 waves of spherical aberration. Figure 11 (b) shows the theoretical maximum surface density of far-field read out systems versus refractive index of the substrate, assuming that the system compensates 2, 10 and 20 waves of spherical aberration. Surprisingly, media with higher refractive index have less effective surface density. This result occurs because Π is proportional to $\frac{n^2}{n^2 - 1}$, which decreases as n increases. Also, Fig. 7 shows theoretical results for λ=405 nm, which indicate maximum Π of 800 Gb/in^2 when $(\Delta W_{040})_{\max} / \lambda$ =20 waves and n =1.5.

Ultra high density near-field systems that use a solid immersion lens (SIL) are also investigated. [18] Figure 12(a) shows the layout of a near-field system. This design exhibits 0.2 mm allowable focus depth with 80% or higher Strhel ratio corresponding to $(\Delta W_{040})_{\max} / \lambda = 3.6$ waves. Numerical calculations are performed to determine Π of this near-field System. The results are shown in Fig 12(b). When λ=633 nm, the maximum surface density reaches 920 Gb/in^2 to 1100 Gb/in^2 for n_{SIL} =1.5 and n_{SIL} =2, respectively, at NA=1.5 and NA=1.9. When λ=405 nm, the maximum surface density can reach 2750 Gb/in^2 and 3300 Gb/in^2 for n_{SIL} =1.5 and n_{SIL} =2, respectively, at NA=1.5 and NA=1.9. For a moderately complex system, like NA=1.2 and n_{SIL} =1.5, Π is 1.8 terabits-per-square inch (1 Tb/in^2=1000 Gb/in^2) at λ=405 nm.

Wavelength-Domain Tracking

To achieve a high data transfer rate, a multiple-beam optical system is investigated. The motivation is the need of individually-addressable multiple-beam sources for simultaneous recording on multiple tracks and adjustability of individual spot spacing on the disk to overcome track pitch variation, track eccentricity and track winding.

A new idea of multiplexing and controlling multiple beams in the wavelength domain is developed. Multiplexing conversion between wavelength and angle domain enables beams to illuminate different tracks on the disk. Furthermore, error signals are extracted in each channel from the multiple beams by low-frequency modulation of individual laser diodes.

A schematic of the wavelength-multiplexed system is shown in Fig. 13. Beams with different wavelengths are multiplexed using a beam combiner and diffracted on a blazed grating at different angles. The angle-multiplexed beams illuminate adjacent tracks on the storage medium. The reflected beams go to servo and data detectors. Since the beams are modulated with a low-frequency with separation of a few kilohertz, error signals are extracted using bandpass filters with no need of separate servo detectors. For data readout, another blazed grating is used to allocate each reflected beam to individual detectors. In case track defects on one of the tracks or track pitch variation cause errors, the system compensates by changing the wavelengths of the corresponding channels individually.

VII. SUMMARY AND CONCLUSIONS

Several aspects of implementing bit-wise volumetric data storage for space applications are reported. An Advanced Engineering Model (AEM) is implemented with an improved servo system. The new servo system should improve the performance of the system in high-temperature environments. The AEM is designed to use a reference track at one laser wavelength and write/read beams at different wavelengths. Multiple-wavelength optical design includes the use of a diffractive optical element (DOE). The system is designed to use inexpensive homogeneous nonlinear recording material. A less-advanced servo system is used with the AEM in preliminary experiments to demonstrate reading and writing high-quality bits in the material. With respect to space-flight environment damage of the material, results indicate that the two-photon material is not sensitive to heavy ions, but it is sensitive to high-energy protons at exposure levels over 20,000 krad. A new test stand for developing volumetric media is described. The new test stand incorporates a spinning head design, and it can test focus sensitivity and pulse-width/power optimization. Channel development results indicate that up to 3.3 Tb/in^2 effective surface density is possible with the media under test if used with an appropriate optical system. Finally, a new multiplexing technique is under development that uses wavelength multiplexing to increase data rate.

ACKNOWLEDGEMENT

This work is supported through a contract from the National Aeronautics and Space Administration, contract # NAS2-00117.

REFERENCES

[1] "Earth Science Enterprise: Strategic Plan," November, 2002, NASA Headquarters Washington, DC 20546, http:// www.earth.nasa.gov

[2] Tom D.Milster, Yan Zhang, J Butz, Tim Miller and E.P.Walker, "Volumetric Bit-Wise Memories**"** Proceedings of the NASA Office of Earth Science (OES) Advanced Information Systems Technology (AIST) Program workshop on projections for future spacecraft needs, Jan 9-10, 2002, Jet Propulsion Laboratories, Pasadena, California.

[3 S. Hunter, F. Kiamilev, S. Esener, D. A. Parthenopoulos, and P. M. Rentzpis, "Potentials of two-photon 3-D optical memories for high performance computing," *Appl. Opt.* **29**, pp. 2058-2066 (1990)

[4] E. W. Van Stryland *et al.,* "Characterization of nonlinear optical absorption and refraction," *Prog. Crystal Growth and Charact.* **27**, pp. 279-311 (1993).

[5] H. Zhang, F. McCormick, A. Dvornikov, C. Chapman, E. Walker and N. Kim *et al.,* "Single-beam two-photon-recorded monolithic multi-layer optical disks," *ODS 2000* Proc. SPIE 4090 pp. 174-178 (2000). [6] E. P. Walker ,W. Feng, Y. Zhang, H. Zhang, F. B. McCormick, S. Esener,, "3-D parallel readout in a 3-D multilayer optical data storage system" Technical Digest of the 2002 international Symposium on Optical Memory and Optical Dat Storage Topical Meeting, Waikoloa, Hawaii, July 7-11, 2002, IEEE Catalog number 02EX552, pp. 147-149.

[7] A. Marchant, "Optical Recording: A Technical Overview", Addison-Wesley Co., New York 1990, p. 181

[8] Tom D. Milster, Robert S. Upton and Hui Luo, "Objective lens design for multiple-layer optical data storage," Optical Engineering 38(2) p. 295-300

[9] Ed Walker *et al.,* "Spherical aberration correction for two-photon recorded monolithic multilayer optical data storage" *Optical Data Storage Topical Meeting* 2001 154-156

[10] . T.J. Suleski and D.C. O'Shea, "Gray-scale masks for diffractive-optics fabrication: I. Commercial slide imagers", Appl. Opt., Vol. 34, No. 32, pp.7507-7517 (1995).

[11] S. Esener and E. P. Walker ," : Present performance and new directions in two-photon addressed volumetric optical storage systems," SPIE Photonics West Conference 2003, Paper 4988-27.

[12] J. Barth, "Ionizing Radiation Environment Concerns" Conference of Single Event Effect Criticality Analysis, http://radhome.gsfc.nasa.gov/radhome/papers/seeca3.htm

[13] For more information of calculating penetration depth http://tvdg10.phy.bnl.gov/LETCalc.html

[14] S. Guertin, G. M. Swift, and D. Nguyen, "Single-Event Upset Test Results for the Xilnx XQ1701L PROM," 1999 IEEE Radiation Effects Data Workshop, pp. 14-21, published by IEEE, Inc.

[15] T. D. Milster, "A user-friendly diffraction modeling program," Optical Data Storage Topical Meeting, Conference Digest, April 7-9, Tucson, AZ 1997, IEEE. 109, pp. 60-71

[16] T. D. Milster, " Physical optics simulation in Matlab for high-performance systems" 3rd International Conference on Optics-photonics Design & Fabrication October 30-November 1, 2002, Tokyo Japan p 15-16.

[17] Robert.S. Upton and Tom D Milster "Detector patterns from optical disks" Optical Engineering, vol 40 No6 June 2001 1030-1044

[18] T.D. Milster, "Near-field optics: A new tool for data storage," *Proc. IEEE*, 88(9), pp 1480-1490 (2000).

Table 1 Test results of the photo-chromic disks after they are exposed to heavy ion radiation.

Particles	Flux (p/cm^2-s)	Fluence (p/cm^2)	Total dose (krad)	Incident Angle	Energy (MeV)	Range (μm)	Failure rate
I-127	1.5e5	2e7	224	0^o,45^o	350	48.62	0%
Br-81	2.5e4	5e6	46	0^o,45^o	290	56.57	0%
Ni-58	3e4	1e7	83	0^o,45^o	260	64.41	0%
Cl-35	1e5	2e7	134	0^o,45^o	210	102.8	0%
Mg-24	2e5	2e7	109	0^o,45^o	170	149.2	0%
F-19	1.2e5	2e7	90	0^o,45^o	140	200.8	0%

Table 2 Test results of the photo-chromic disks after they are exposed to proton radiation.

Energy (MeV)	Flux (p/ cm^2-s)	Total dose (krad)	Radiation period (s)	Failure rate
30	1e6	9.6	10	0%
30	1e6	48	50	0%
30	1e6	96	100	0%
30	1e9	9.6e3	10	100%
30	1e9	4.8e4	50	100%
30	1e9	9.6e4	100	100%
60	1e6	19.2	10	0%
60	1e6	96	50	0%
60	1e6	192	100	0%
60	1e9	1.92e4	10	100%
60	1e9	9.6e4	50	100%
60	1e9	1.92e5	100	100%

Table 3 Focus spot speed versus data rate versus minimum power required for sample 1

Focus spot speed	Data rate	Minimal power required
1m/s	250 KHz	1.5 mw
	120 KHz	1.5 mw
2m/s	500 KHz	2.5 mw
	250 KHz	2.5 mw
3m/s	750 KHz	3.5 mw
	375 KHz	3.5 mw
4m/s	1 MHz	4.5 mw
	500 KHz	4.0 mw

Table 4 Focus spot speed versus data rate versus minimum power required for sample 2

Focus spot speed	Data rate	Minimal power required
1m/s	250 KHz	12 mw
	120 KHz	11 mw
2m/s	500 KHz	15.5 mw
	250 KHz	15.5 mw
3m/s	750 KHz	*
	375 KHz	*
4m/s	1 MHz	*
	500 KHz	*

*: beyond the maximum output power of the laser used in this test stand

Table 5 Simulation results of focus sensitivity for both confocal (v_d=0.9) and non-confocal (v_d=8) systems. NA=0.6.

L_x=L_y (μm)	L_z (μm)	Detector	SNR(dB) at $\Delta z = L_z/2$	Δz_0 (μm)
0.5	0.9	confocal	28.0	2.0
		non-confocal	33.7	3.5
	1.8	confocal	30.5	2.3
		non-confocal	36.5	3.6
	2.7	confocal	31.4	2.84
		non-confocal	38.0	3.8
1	0.9	confocal	28.5	2.0
		non-confocal	35.7	3.5
	1.8	confocal	31.3	2.3
		non-confocal	38.5	3.6
	2.7	confocal	32.1	2.84
		non-confocal	40.0	3.8
1.5	0.9	confocal	28.5	2.0
		non-confocal	35.7	3.5
	1.8	confocal	31.3	2.3
		non-confocal	38.6	3.6
	2.7	confocal	32.1	2.84
		non-confocal	40.2	3.8

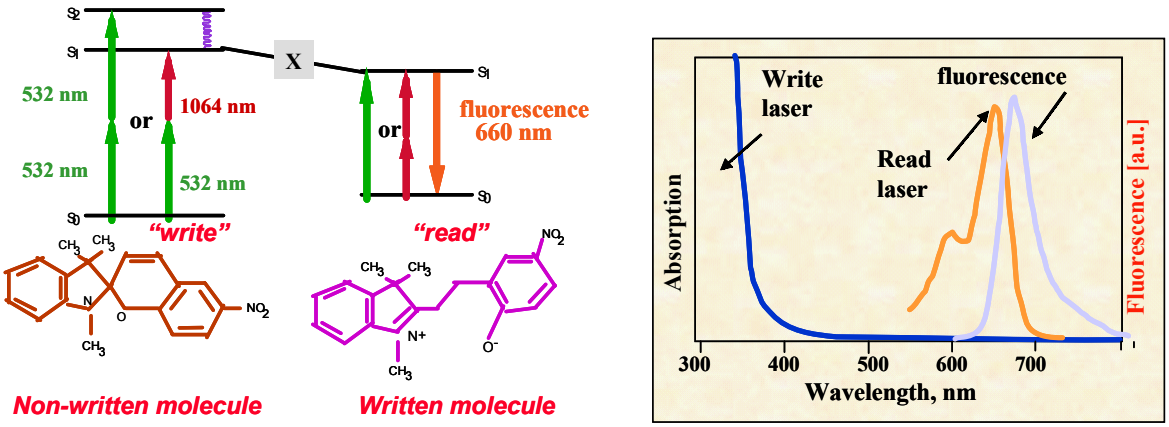

Figure 1 A physical description of what happens when two-photon absorption occurs. The left one is the energy-level diagram and molecular structure of unwritten and written forms, showing fluorescence. The right one is the absorption spectra and fluorescence spectrum of the unwritten and written forms of the material

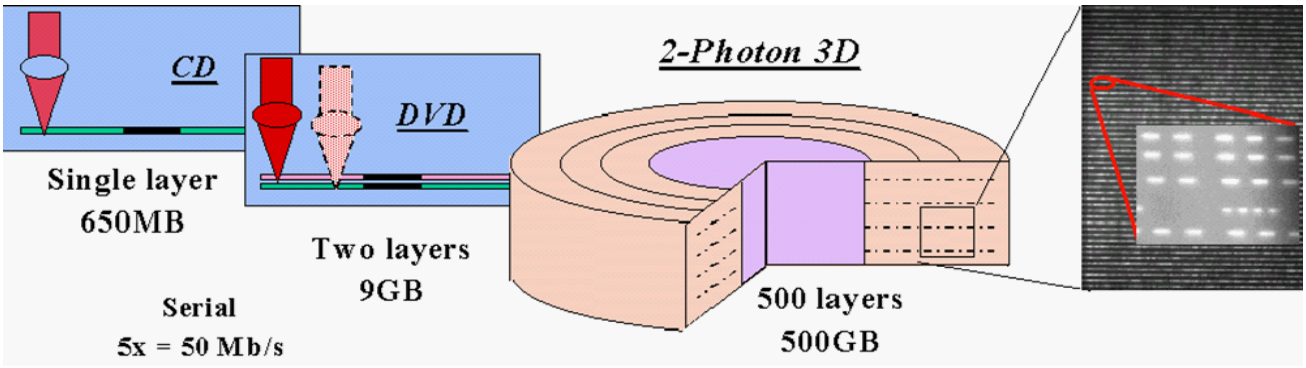

Figure 2 The comparison between a CD, a DVD and a volumetric storage system.

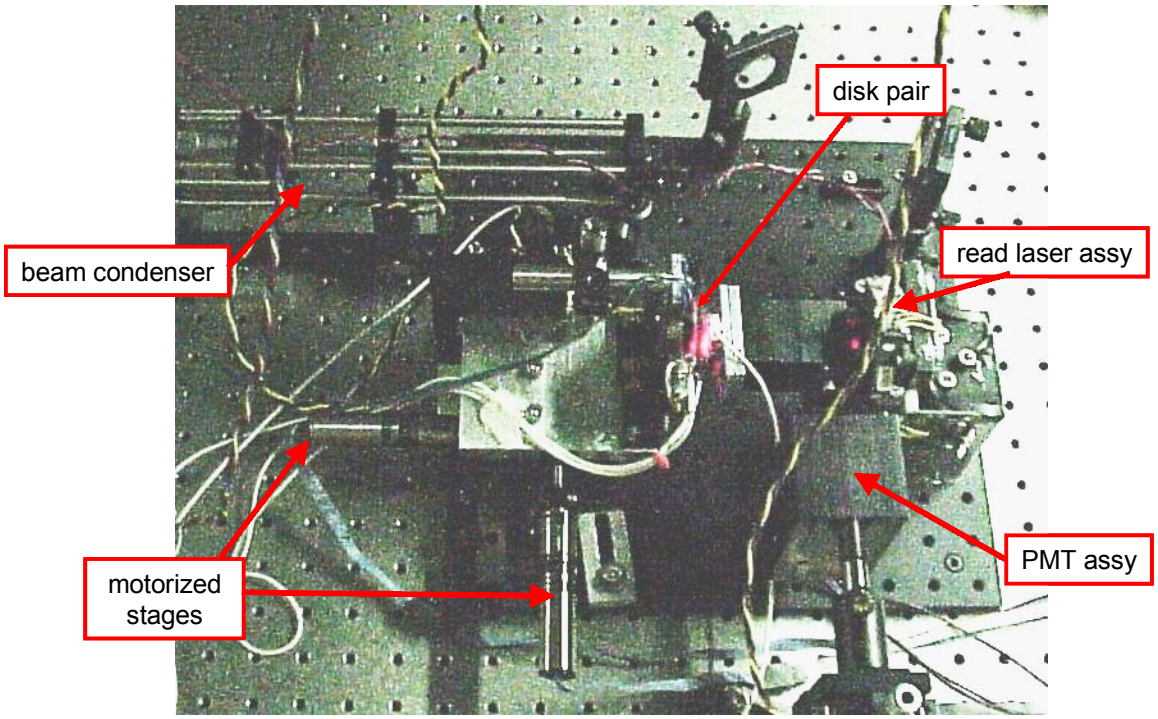

Figure 3 The Advanced Engineering Model. A commercial CD-R and a 3"-diam. Call-Recall medium are mated with optical adhesive to form a rigid disk pair. The writing, reading and tracking beams are combined through a beamsplitter block and are focused through our objective into the medum.

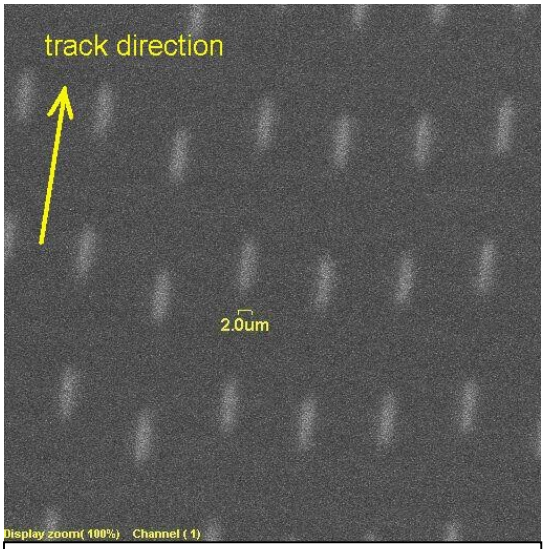

Figure 4 A confocal microscope shows a series of single-frequency

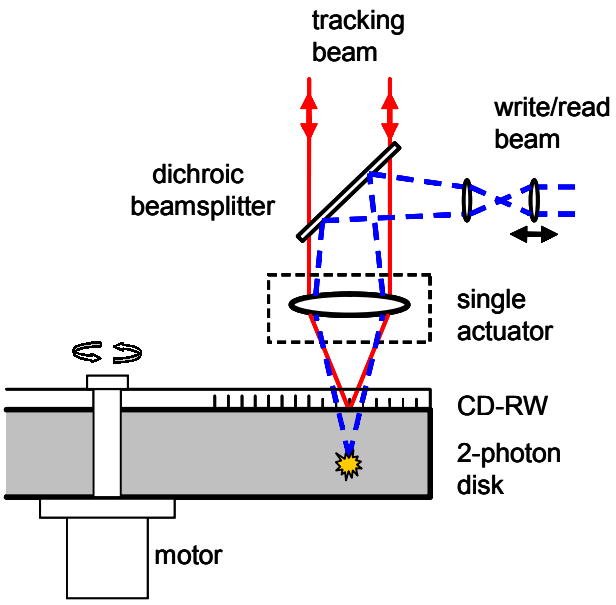

Figure 5 The two-in-one configuration combines the tracking beam and the write/read beams into a single path.

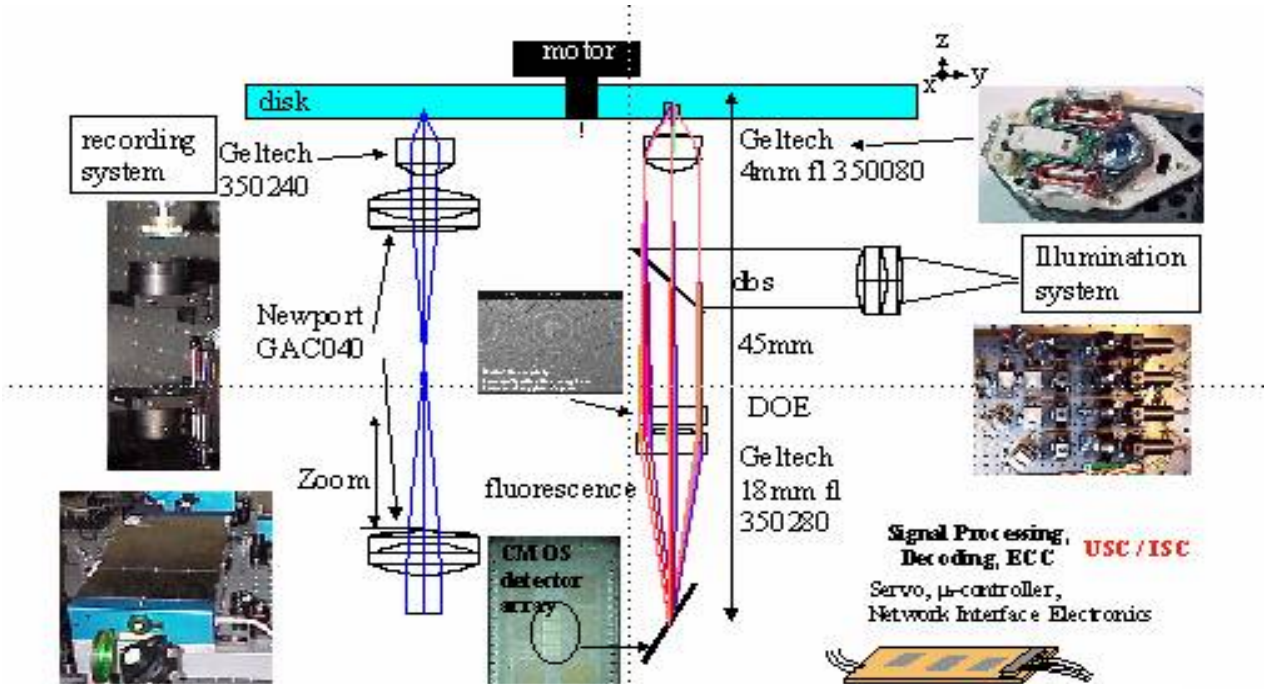

Figure 6 Experimental optical system architecture showing the separate recording and readout heads allowing independent recording and readout experiments (combined recording/readout heads are designed). The recording head has adjustable spherical aberration for recording throughout the disk thickness. The DTO layout indicates various system components such as the Parallel Solutions, Inc. 64 channel detector array, the reconfigurable fpga signal processing encoding/decoding developed by USC and Irvine Sensors, Inc, and the various optical system components

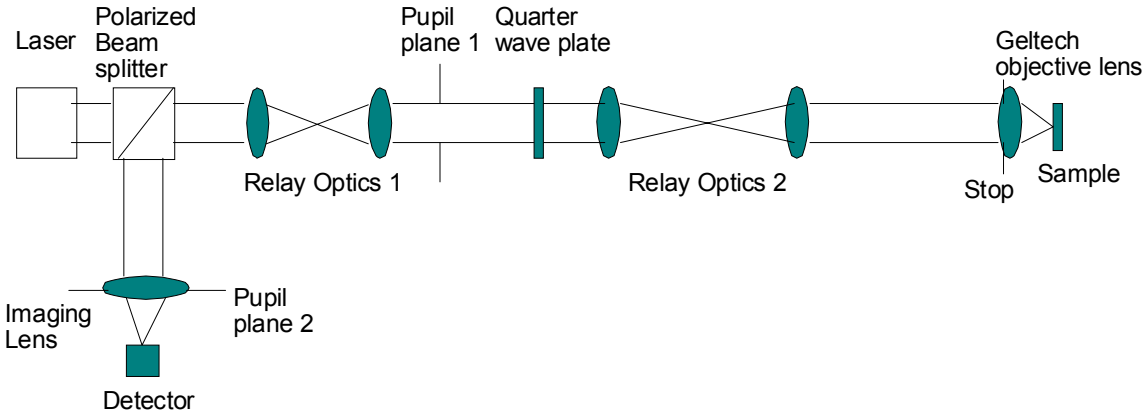

Figure 7 The setup of the dynamic test stand, which is used to test coupon samples.

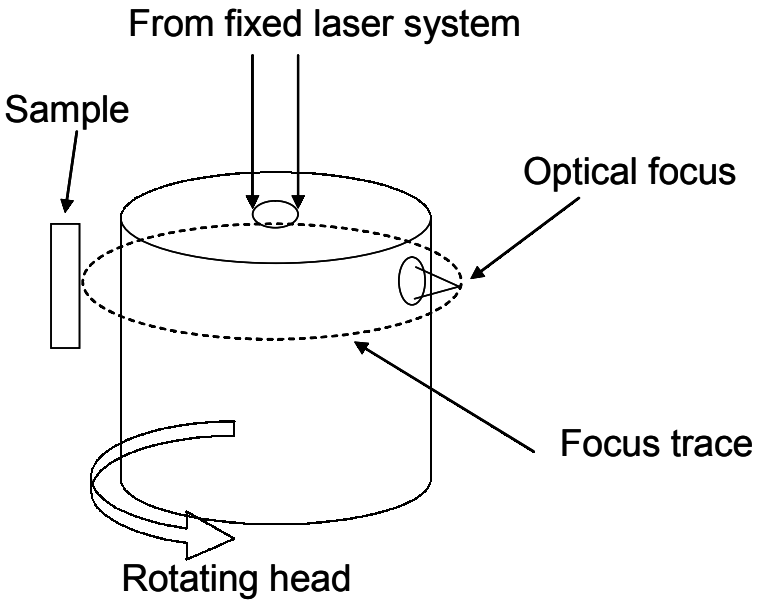

Figure 8 The optical head and the coupon sample

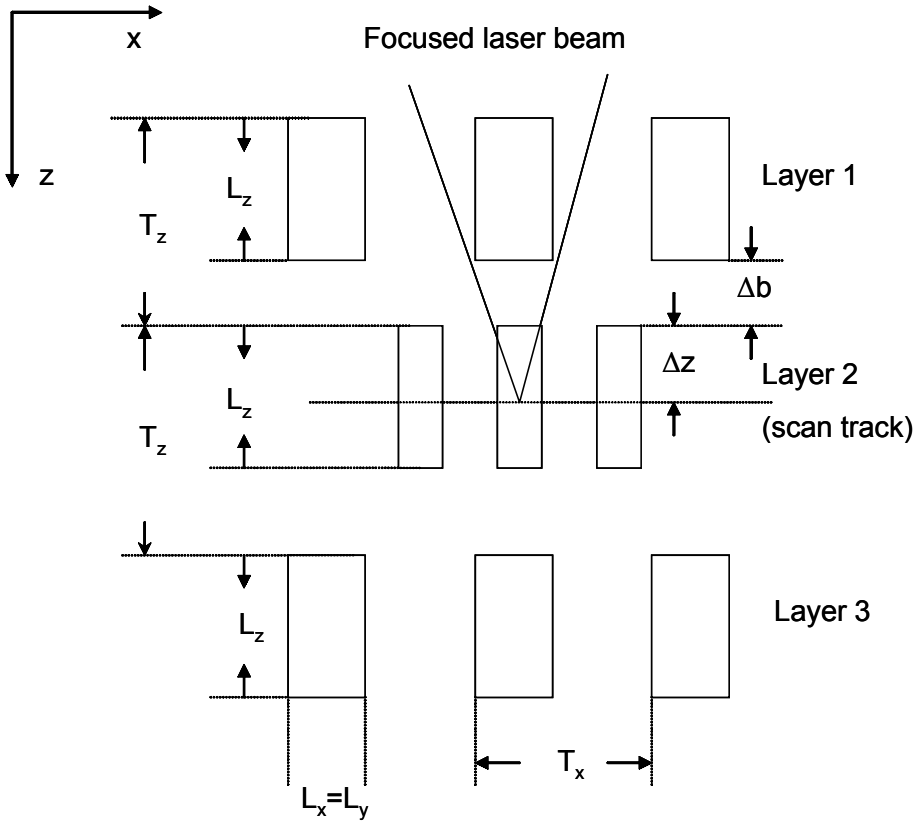

Figure 9 Mark patterns used to simulate inter-layer crosstalk. Layer 2 contains the scan track. Mark depth is L_z. Layer 2 contains high-frequency data marks, while Layer 1 and Layer 3 contain a larger, low-frequency data marks. The offset of the focus beam from the top of Layer 2 is Δz. Δb is the spacing between data mark layers.

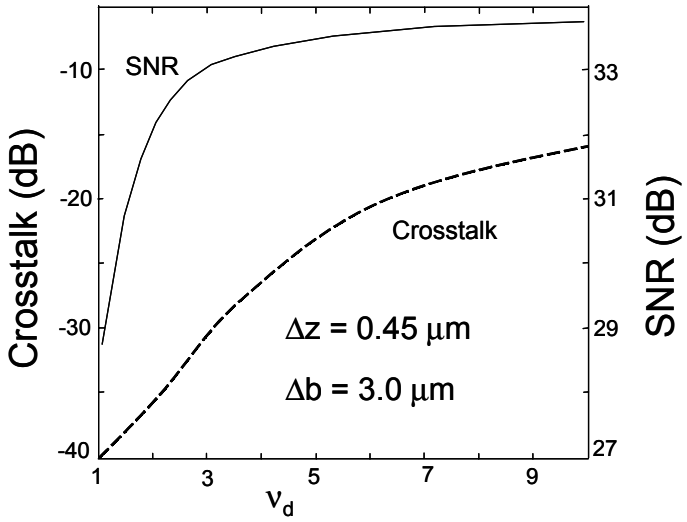

Figure 10 Inter-layer crosstalk level and SNR versus normalized detector radius for a system with $\Delta z = 0.45$ μm and Δb = 3.0 μm. NA=0.6, λ=633nm.

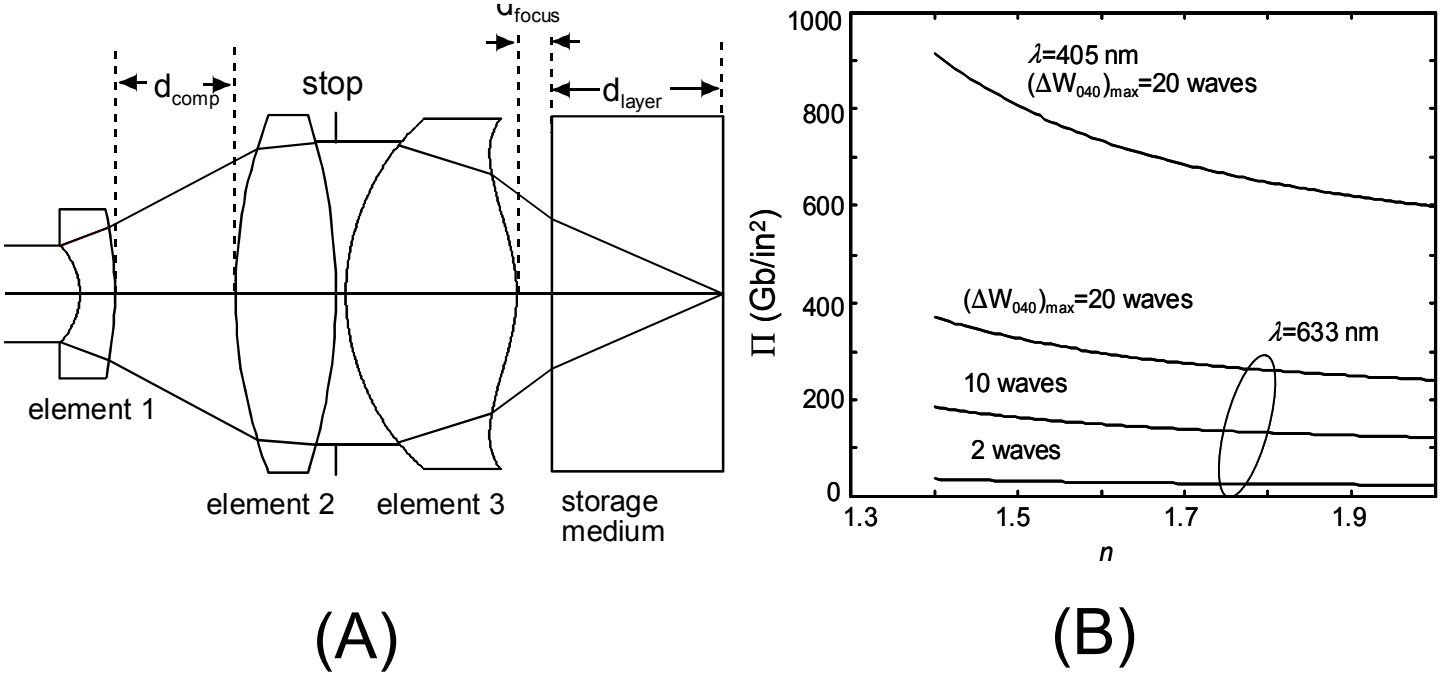

Figure 11 (a) Layout of a far-field system designed for optimum compensation through volumetric media. The lens elements extend over a track length of only 13mm. d_{focus} is adjusted to change data layers, and d_{comp} is changed to adjust for spherical aberration. (b) Effective surface density Π of a far-field read-out system versus medium refractive index when (a) λ=633nm, $(\Delta W_{040})_{max}$ = 20 waves; (b) λ=633nm, $(\Delta W_{040})_{max}$ = 10 waves; (c) λ=633nm, $(\Delta W_{040})_{max}$ = 2 waves; and (d) λ=405nm, $(\Delta W_{040})_{max}$ = 20 waves.

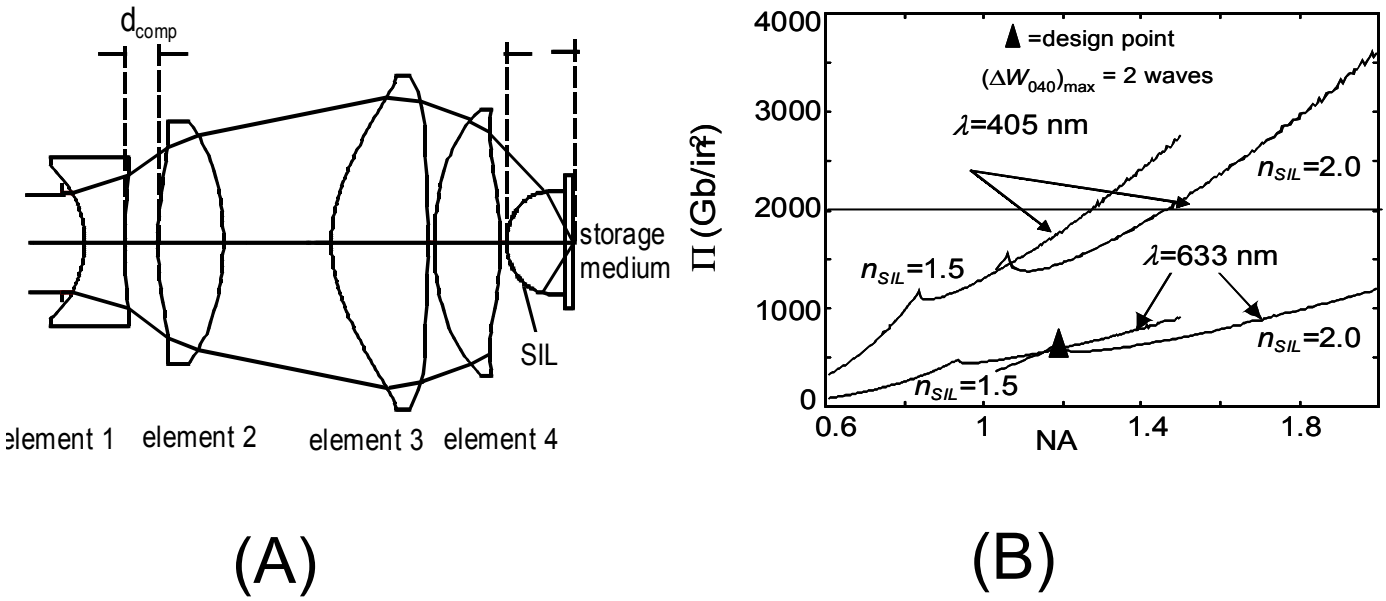

Figure 12 (A) Layout of a Near-field System. (B) Effective surface density Π of the Near-field System versus NA when (a) λ=405nm, *n*=1.5; (b) λ=405nm, *n*=2.0; (c) λ=633nm, *n*=1.5; (d) λ=633nm, *n*=2.0.

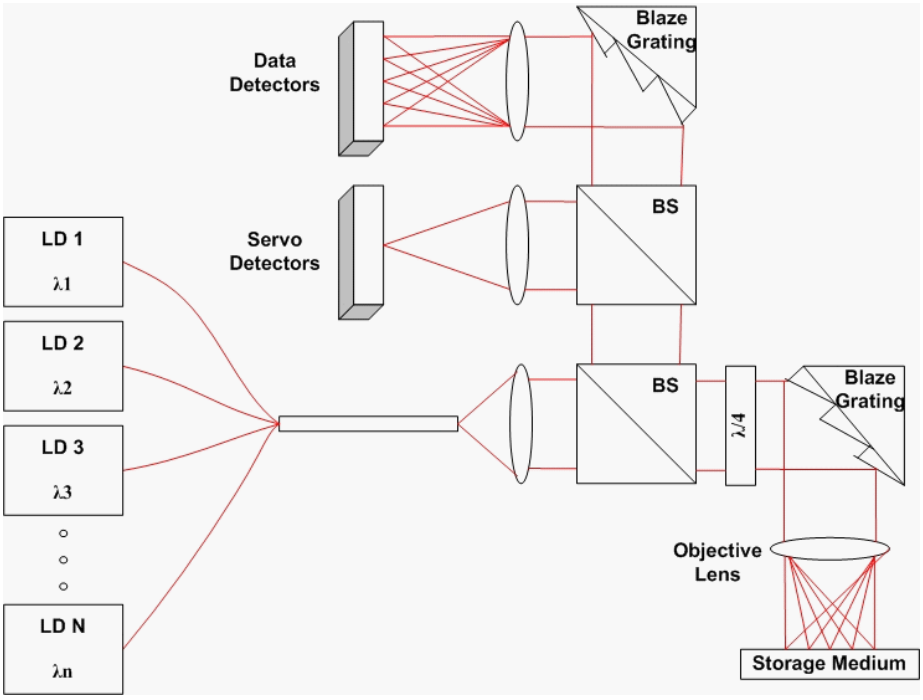

Figure 13 A schematic of the wavelength-domain tracking system. Multiple beams with different wavelengths are generated by tunable laser diodes and multiplexed into a combiner. After passing a beam splitter and a quarter-wave plate, the multiplexed beam hits a blazed grating where multiplexing conversion occurs from wavelength domain to angular domain. The angularly distributed beams illuminate separate tracks and reflect back to the grating. The recombined beam goes to data and servo detectors. Wavelength tunability in laser diodes and multiplexing conversion on the blazed grating are the key factors in wavelength-domain tracking